Hindawi
Advances in Civil Engineering
Volume 2021, Article ID 8899685, 14 pages
https://doi.org/10.1155/2021/8899685

Research Article

A Quantitative Evaluation Method Based on Back Analysis and the Double-Strength Reduction Optimization Method for Tunnel Stability

Jinglai Sun, Fan Wang, Xinling Wang, and Xu Wu

Beijing Municipal Engineering Research Institute, Beijing 100044, China

Correspondence should be addressed to Xu Wu; 13051510807@163.com

Received 4 September 2020; Revised 19 October 2020; Accepted 19 February 2021; Published 12 March 2021

Academic Editor: Alessandro Palmeri

Quantifying tunnel stability using the proposed combination of back analysis and the strength reduction method (SRM) is useful during construction. To feasibly and reliably obtain geotechnical parameters for the surrounding rock (which vary in different places), a real-coded genetic algorithm is used in setting the initial parameters of the neural network to improve the prediction accuracy of the parameters via back analysis by reasonably selecting the selection operator, crossover operator, and mutation operator. After obtaining the parameters, the proposed SRM, i.e., the optimization double-strength reduction method (ODSRM), which is based on the optimization method, is used to evaluate stability. By using this method, the cohesion and friction angle have different reduction factors that are more reasonable and accurate. The combined method is verified in an application to the Yu Liao Tunnel, where it is demonstrated that the combined method can use the measured displacements to obtain the safety factor. Compared with the traditional method, the proposed back analysis method can reduce errors in the predicted performance, and unlike the SRM, the ODSRM can avoid overestimating the safety factor with the same reduction factor. Finally, the presented methods can reduce the amount of calculation required and are convenient for evaluating tunnel stability with displacement.

1. Introduction

The quantitative analysis of stability is very important during tunnel construction [1]. The strength reduction method (SRM) is traditionally used to assess slope stability [2–6] and in tunnel stability analysis [7–10]. The SRM was first proposed by Zienkiewicz et al. [11] in 1975 and has been applied by Matsui 2, Michalowski [12], Naylor [13], and others.

In the traditional SRM, the cohesion c and friction angle φ are reduced by the same reduction factor; for this approach, the cohesion and friction angle are treated identically as damage to the engineered structure is gradually accrued. However, according to some researchers [14–17], the two indices have different effects and reduction rates in the destabilization process. To address this issue, many scholars have adopted the double-strength reduction method (DSRM), which separately reduces the cohesion and friction angle by different coefficients. For example, the shortest path of strength reduction was proposed by Isakov and Moryachkov [18], Wang has applied this method to shallow buried tunnels [19], and Yuan [20] and Bai [21] each studied the DSRM.

Rock mass characteristics have significant effects on the stability of the tunnel through the rock mass; however, the values of the rock mass parameters are very difficult to determine in practice, and the use of inaccurate values directly affects stability analysis. Although in situ measurement is the most popular method for obtaining these values, it consumes considerable resources and time and can be conducted only in certain engineering projects [22, 23]. To obtain these values feasibly and reliably using limited amounts of measurement data, the most commonly used and efficient method is called back analysis to infer "cause" from "result" [24, 25]. The back analysis in geotechnical engineering can be divided into displacement back analysis, stress back analysis, strain back analysis, and groundwater

seepage field back analysis. Displacements are often measured because of their reliability and convenience; thus, back analysis based on displacements has been studied by many scholars [26–30]. Artificial neural networks (ANNs) are typically used in back analysis and can provide an appropriate approach to representing the nonlinear relationship between rock mass characteristics and displacements [31].

ANNs are made up of many neurons, which reflect the intensity of their connections through weights, and many neurons connect with each other to form complex neural networks. Because of the different types of neurons, the means of connection and the means of learning, ANNs can be divided into many types. The BP-ANN is an algorithm based on the least-squares method, which is realized by minimizing the mean square error between the output value and the expectation of an ANN. Before the error threshold is reached, the network is constantly iterative, and each iteration includes the forward propagation of information and the reverse propagation of error. As shown in Figure 1, datasets u, e, and y are used as samples of input and output, and multiple sets of training data can be collected to train neural networks. Before training, the weight of the network is initialized by a random number. The input data are calculated and processed by the input layer, the hidden layers, and the output layer to obtain the output data. The output data are then compared with the expectation to gain the mean square error, and the inverse propagation stage of the error is conducted until the error is satisfied. During the process, the weights between the neurons of each layer are adjusted. The function of the error decreases along the direction of negative gradient. The iterations continue according to the above steps until the final error is less than the threshold or the number of iterations reaches the upper limit to stop the training. The weight value after training is used as the final weight of the neural network, and the neural network can be used for back analysis and calculation. To search for estimated parameter values in a large space, the genetic algorithm (GA) and the simulated annealing technique are the often used algorithms of greatest efficiency [32, 33].

However, conventional GAs are prone to low computational efficiency or local optimal value problems, so it is necessary to improve the efficiency of back analysis and calculation and avoid the emergence of a local optimal value. In the present paper, the real-coded genetic algorithm (RCGA), which is better than GA due to its binary code and is seldom used in the back analysis of geotechnical parameters [34], is selected to determine the initial parameters of an ANN. To avoid a local optimal value and increase computational efficiency, the selection operator, crossover operator, and mutation operator are recombined. The proposed approach can be used to determine the weight value of an ANN and is called the RCGA-ANN.

Therefore, a new DSRM, coupled with the back analysis, is proposed to evaluate the stability of a tunnel. An optimization method, called the mode search method, is used to iteratively search for reasonable values for the two indices; this approach, called the optimization double-strength reduction method (ODSRM), does not require much calculation or a fixed proportion, which are commonly encountered issues of the shortest-path method. This paper presents the details of a new approach for calculating the indices to evaluate tunnel stability.

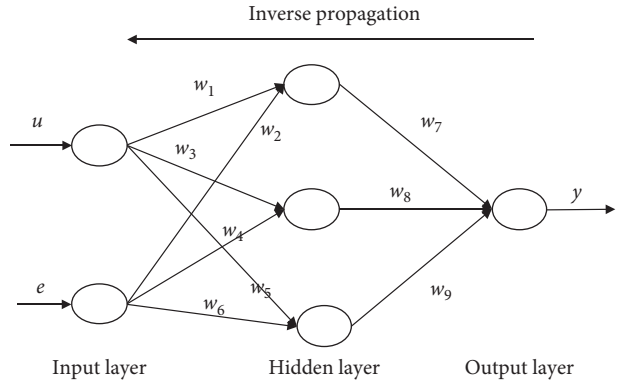

Figure 1: Structure of a BP-ANN.

A combination of the RCGA-ANN and ODSRM is proposed to feasibly and reliably obtain geotechnical parameters for the surrounding rock and evaluate the stability of the surrounding rock. The descriptions of the methods are provided as follows.

2. Displacement Back Analysis Based on the RCGA

Displacement back analysis can be a convenient approach for determining rock mass characteristics, which are difficult to determine via field measurement [22, 35, 36]. Uniform design [37] is used to obtain the training samples for back analysis. In this paper, to improve the performance by solving a shortcoming of an ANN (i.e., that the characteristics of a local minimum could be obtained) [38], the RCGA is used to determine initial network weights; this approach is called the RCGA-ANN.

2.1. Method Improvement. The main purpose of this section is to propose an efficient hybrid GA based on the RCGA. This method can be used in the process of building the ANN to obtain the reasonable connection weights, has high computing efficiency, and avoids local optimal values. The characteristics of this method can be used to identify the geological parameters.

In a traditional GA, each variable in an individual is generally represented by the binary digits 0 and 1. This encoding method performs well in solving problems with low precision or low dimension, but it takes a long time to calculate and requires a sophisticated computer configuration for problems with high precision or high dimension. Because each variable is represented by real numbers in the RCGA, this method can be used to solve this problem, which has been widely applied and considered. In particular, when addressing the optimization of continuous space, the RCGA is obviously superior to GA binary coding [38].

This section primarily develops a hybrid GA based on real-number coding to optimize the network weight

parameters of the neural network back analysis method. Based on the traditional GA, to avoid local optimization and improve computational efficiency, the hybrid algorithm is used to select the population by using the sorting selection method. Two newer crossover operators are fused to form a new crossover strategy. To ensure the diversity of the population, a dynamic stochastic mutation operator is selected in the algorithm.

Because the initial weights of neural networks are generated by random numbers, the final weights may lead to a local optimal value. The RCGA is introduced in this paper to optimize the weights of neural networks. The obtained neural network is embedded by the RCGA, which assists in the back analysis. The main ideas are as follows: (1) the weight parameters of the neural network are trained repeatedly using the training dataset to produce the initial population (each individual is one combination of the weight value of the neural network); (2) each individual is taken as the weight value of the neural network to calculate the fitness of the testing dataset; (3) the contemporary population is determined via selection, crossover, and mutation operations, due to the corresponding probability and calculation factors, to obtain a new population; and (4) an iterative calculation is performed until the adaptability of the population can meet the expected standards. Because the next generation of stocks can inherit the excellent characteristics of the parent generation, the overall evolution of the population tends to the optimal solution. The calculation process for this method is shown in Figure 2, and the calculation steps are as follows:

(i) *Step 1.* Initial network weights are determined via the RCGA. At the beginning of the RCGA, the generation with $P(g)$ individuals (i.e., with $P(g)$ choices of initial network weights in the ANN) is randomly generated, where g is the iteration or generation with $g = 0$.

(ii) *Step 2.* Based on the networks obtained via the training samples, the ANN reads in the training samples, testing samples, and initial network weights (for network training by the training samples) and predicts the testing samples. The fitness of the predicted results is then evaluated according to the given adaptation function.

(iii) *Step 3.* The individuals undergo reproduction, crossover, and mutation operations according to their fitness, and the individuals of the new generation, $P(g+1)$, are obtained. The generation is $g = g + 1$.

(iv) *Step 4.* Determine whether a predetermined evolutionary number (PEN) is reached (e.g., by reaching the end of a calculation) and return the individual with the highest fitness; otherwise, return to *Step 3* until the termination condition is satisfied.

(v) *Step 5.* Obtain the optimization parameters of the networks.

2.2. Selection Operation. Roulette wheel selection (RWS) and tournament selection (TS) are the two approaches most frequently used in the RCGA. However, RWS is slow because of the heavy computation required in each generation, and TS can miss potential solutions and obtain a local optimum. Ranking selection (RS) is used in this paper because it has the benefits of the above approaches but is more efficient [39].

First, individuals are ranked by their fitness. Then, $\lfloor pN \rfloor$ low-ranking individuals are discarded, and $\lfloor pN \rfloor$ high-ranking individuals are generated; p is a proportional parameter in interval $(0, 0.5]$. The RS function is illustrated in Figure 3 on a population of eight individuals with respect to various proportions. The population size is from 10 to 200.

2.3. Crossover Operation. By combining the advantages of various crossover operators, the search ability of the new RCGA can be improved [38]. We selected two real-coded crossovers: the simulated binary crossover (SBX) [40] and directed crossover (DCX) [41]. Crossover probabilities (P_c or P_s) are used to select a crossover from 0 to 1.

Based on relevant research [40], the search power and performance of the SBX used in the real-coded algorithm are better than those of the single-point crossover used in the binary-coded algorithm. The steps of the algorithm are as follows:

$$\xi_i = 0.5\left[(1+\beta_i)x_i^1 + (1-\beta_i)x_i^2\right],$$

$$\eta_i = 0.5\left[(1-\beta_i)x_i^1 + (1+\beta_i)x_i^2\right],$$

$$\beta_i = \begin{cases} (2u)^{1/(\eta+1)}, & \text{if } (u \le 0.5), \\ \left\{\dfrac{1}{[2(1-u)]}\right\}^{1/(\eta+1)}, & \text{if } (u > 0.5), \end{cases} \tag{1}$$

where ξ_i and η_i are two offspring individuals obtained using the SBX, β_i is the spread factor, u is a uniform random number in the range of [0, 1], and x_i^1 and x_i^2 are two parent individuals produced by the selection function. In this paper, η equals 20 [42].

To improve the accuracy of the solution, the directed crossover operator is introduced because it can conduct a local search among the best individuals of the current generation. X_h is an individual selected at random.m individuals that are better than X_h are selected. X_c is the centroid of the m individuals selected and is calculated as follows:

$$X_c = \frac{1}{m}\sum_{i=1}^{m} X_i, \tag{2}$$

where m is the number of individuals that are better than X_h.

New offspring X_n is randomly generated by equation (3):

$$X_n = X_c + \alpha \cdot S_c, \tag{3}$$

$$S_c = X_c - X_h, \tag{4}$$

where α is a random number between 0 and 1.0.

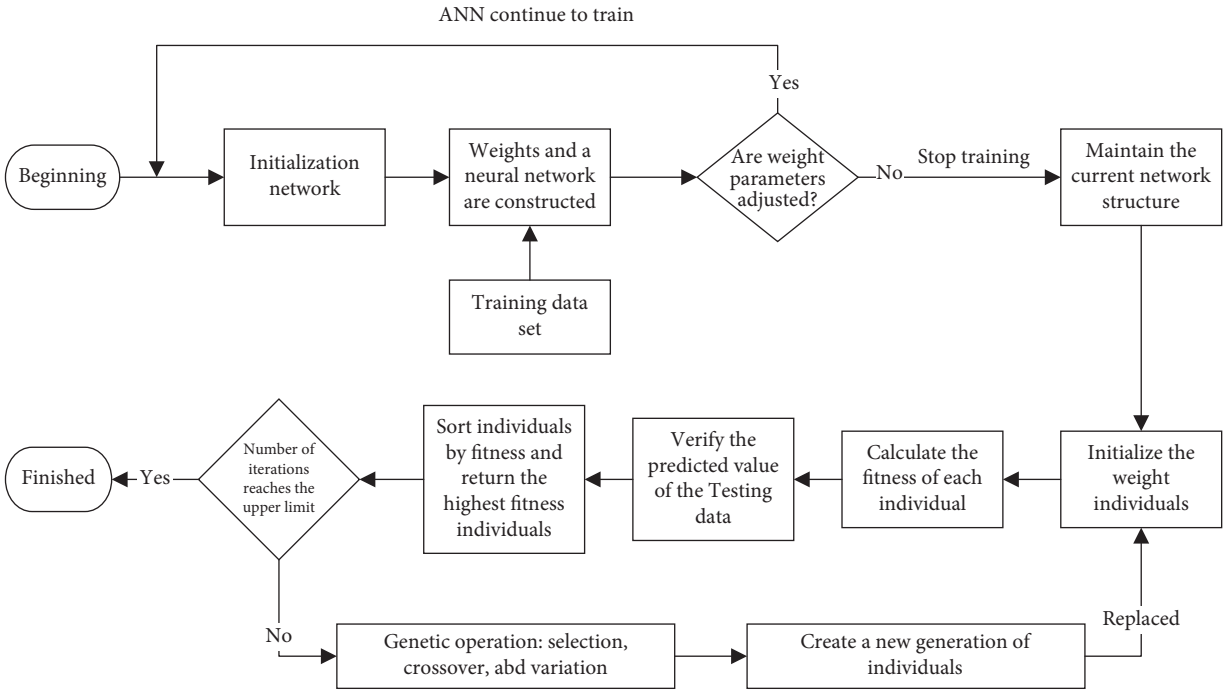

Figure 2: Flowchart of the GA.

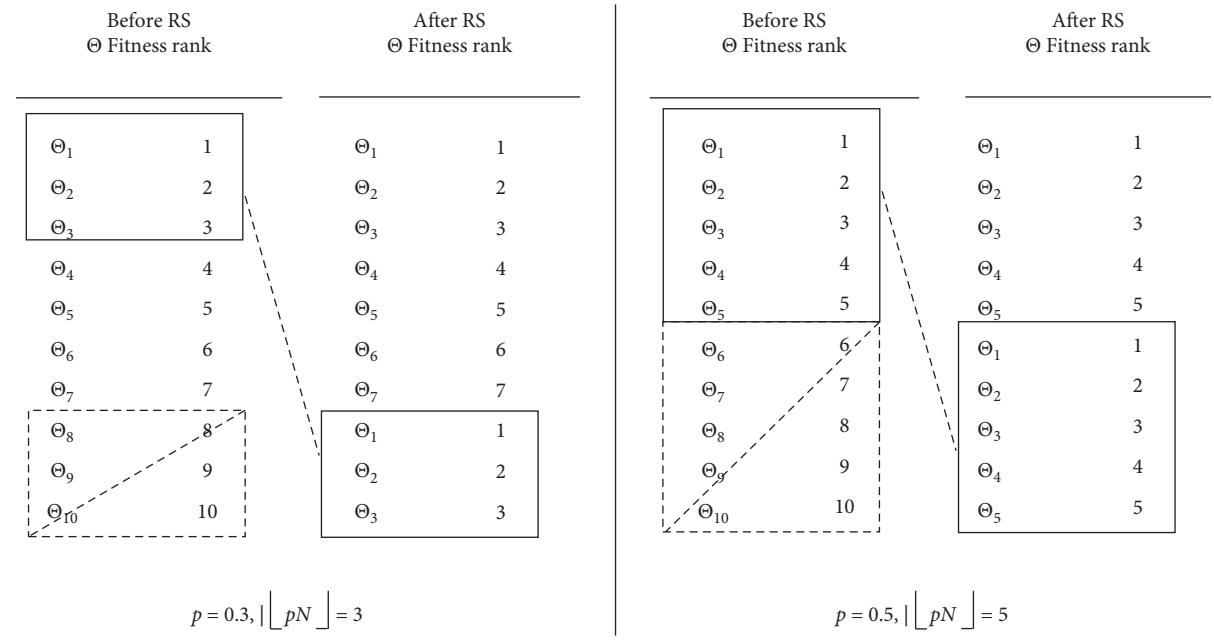

Figure 3: Demonstration of the RS operator with $p = 0.3$ and. $p = 0.5$.

2.4. Mutation Operation. To prevent the population from converging to a local optimum, an excellent new mutation operator—that is, the dynamic random mutation operator (DRM)—is used in the algorithm [39]. The probability of mutation P_m is from 0.0001 to 0.1.

$$X_i^* = X_i + s_m \Phi_0 \left(X^U - X^L \right), \tag{5}$$

where X_i^* is the offspring after mutation; X^U and X^L are the upper and lower bounds of the optimization variable, respectively; Φ_0 is a random perturbation vector of n-dimensional space $[-\phi_0, \phi_0]^n$; ϕ_0 is a user-specified number in the range of $(0, 1]$; and s_m is the mutation step size obtained using equation (6):

$$s_m = \left(1 - \frac{k}{k_{\max}}\right)^b, \tag{6}$$

where b is the decay rate parameter of s_m and k and $k_{\max}$ represent the current generation number and maximum generation number, respectively.

2.5. Fitness Computation. The training error of the individual is used as the fitness function to illustrate the difference between experimental values and the corresponding quantities obtained via the finite element module (FEM); it is defined as

$$f(x) = \sqrt{\frac{1}{n}\sum_{i=1}^{n}\left(\frac{Y^i_{\text{num}} - Y^i_{\text{exp}}}{Y^i_{\text{exp}}}\right)} \times 100, \tag{7}$$

where n is the number of test values, Y^i_{exp} is the ith experimental value of the measurement points, and Y^i_{num} is the ith numerical value of the measurement points.

$$\text{Fit}(f(x)) = \frac{1}{1 + c + f(x)}, \quad c \geq 0 \; c + f(x) \geq 0, \tag{8}$$

where c is a conservative estimate of $f(x)$. In this paper, c equals 0.

3. Optimization of the Double-Strength Reduction Method

3.1. Optimization of the Double-Strength Reduction Method. Assume that the use of the Mohr-Coulomb failure criterion and the characteristic strength properties of the cohesion c and friction angle φ undergo a subsequent incremental decrease to c' and $\tan\varphi'$, respectively.

The stability of the surrounding rock of a tunnel is considered to be affected by a combination of c and φ; that is, when either c or φ loses function, the other index acts as a form of resistance. The surrounding rock becomes unstable only when neither of the two indices can resist the sliding force.

Using the Mohr-Coulomb failure criterion in the tunnel project, the shear strength indices, c and $\tan\varphi$, are separately reduced, as shown as equation (9):

$$\begin{aligned} c' &= \frac{c}{k_1}, \\ \tan\varphi' &= \frac{\tan\varphi}{k_2}, \end{aligned} \tag{9}$$

where k_1 is the reduction factor of c, k_2 is the reduction factor of $\tan\varphi$, c' is the factored cohesion, and φ' is the factored friction angle.

Two issues should be solved in the DSRM: (1) separately reducing c and $\tan\varphi$ and (2) calculating F_s. Theoretically, there are an infinite number of shear strength $(c', \tan\varphi')$ values; thus, the purpose of this paper is to propose an approach with fewer calculations to obtain the only reasonable shear strength $(c', \tan\varphi')$.

Based on Pan Jiazheng's extremum principle [43] and the Hooke-Jeeves algorithm [44], a direct search algorithm, the ODSRM, is proposed. The characteristic strength properties, cohesion c and friction angle φ, which are followed by an incremental decrease in c' and $\tan\varphi'$, are obtained using the method summarized as follows:

(i) Initialization step.

(ii) Let $u_1, u_2, \ldots, u_n$ be the coordinate direction. Choose scalar $\varepsilon > 0$ (to terminate the algorithm), initial step length $\Delta > 0$, and starting point $X^{(0)} = [x_1^{(0)}, x_2^{(0)}, \ldots, x_n^{(0)}]$. Set $Y^{(0)} = X^{(0)}$ and $k = j = 1$. Then, go to the main step.

(iii) Main step

Step a: if $f([x_1^{(k)}, x_2^{(k)}, \ldots, x_j^k - \Delta x_j^{(0)}, \ldots, x_n^{(k)}]) < f(X^{(k)})$, then the trial is a success; let $x_j^{(k+1)} = x_j^{(k)} - \Delta x_j^{(k)}$, and go to Step b.

Step b: if $j < n$, then j is replaced by $j + 1$, and Step a is repeated. If $f([x_1^{(k)}, x_2(k), \ldots, x_j^{(k)} - \Delta x_j^{(0)}, \ldots, x_n^{(k)}]) < f([x_1^{(k)}, x_2^{(k)}, \ldots, x_{j+1}^{(k)} - \Delta x_{j+1}^{(0)}, \ldots, x_n^{(k)}])$, then set $Y^{(k)} = [x_1^{(k)}, x_2^{(k)}, \ldots, x_j^k - \Delta x_j^{(0)}, \ldots, x_n^{(k)}]$; otherwise, go to Step c.

Step c: let $X^{(k+1)} = Y^{(k)}$. If $(|f(X^{(k+1)}) - f(X^{(k)})|/\Delta) > \varepsilon$, then stop; $X^{(k)}$ is the solution. Otherwise, replace k with $k + 1$, set $j = 1$, and repeat Step a.

In the above, *Steps a* and *b* describe an exploratory search, and *Step c* is used to determine whether to terminate or continue the algorithm.

3.2. Definition of Safety Factor. According to the research of Bai [45] regarding the definition of the DSRM, the safety factor of SRM (F_s) can be represented by reduction factor k as follows:

$$F_s = k = \frac{\tau}{\tau'}, \tag{10}$$

where the shear strength of the geotechnical materials is denoted as τ, and the shear strength under the limit state after reduction is denoted as τ'.

3.3. Instability Criterion. The instability criteria used in the SRM are classified into three main categories [20]: (1) the displacement discontinuity of the characteristic measured location; (2) the interpenetration of the plastic zone; and (3) the divergence of the finite element model iteration. In this paper, the displacement discontinuity is selected as the instability criterion.

4. Constructing the Numerical Calculation Model

4.1. Engineering Background. The Yu Liao Tunnel, one of three long tunnels designed in the Yong-Tai-Wen (Ningbo-

Taizhou-Wenzhou) Expressway, has a 5870 m left tunnel and a 5865 m right tunnel. This tunnel is located in a hilly region with complex geology. The entry section is shallowly covered by a residual body and weathered bedrock with a loose structure. The level of the surrounding rock in the entry section is level V. For the main body of the tunnel, the geology is optimal because the amount of underground water is low (i.e., the main level of the surrounding rock is level III).

According to the relevant requirements, one inclined shaft is located in each tunnel (i.e., left and right) to divide the main tunnel into two sections for construction. Two inclined shafts are located on the right side of the tunnel. The length of number 1 is 520 m, the shaft intersects the left hole at ZK 365 + 317.8, and the right hole horizontal intersection is at YK 365 + 310. The length of number 2 is 550 m, and the shaft intersects the left hole at ZK 365 + 357.8 and the right hole at YK 365 + 350. The layout of the tunnel is shown in Figure 4.

4.2. Field Measurement. The total station is used to measure the construction process of the tunnel. The total station of the V-grade surrounding rock is 10 m per monitored section, that of the IV-level surrounding rock is approximately 30 m per monitored section, and that of the III-level surrounding rock is approximately 50 m per monitored section. A survey point of each section is arranged at the preset point section after tunnel excavation and at the test pile buried in B, C, D, and E, as shown in Figure 5.

4.3. Construction of the Finite Element Model and the Material Parameters. The section located at ZK 362 + 400 is selected to build the FEM. This point is in a region with low mountain slopes and is covered with boulders of approximately 2–4 m in thickness. The compressive strength R_c ranges from 61.1 to 72.5 MPa, with a mean value of 66.8 MPa. The surrounding rock is tuff. The search scopes of the five unknown parameters are shown in Table 1.

GTS NX is used to construct the FEM; the size of the tunnel is shown in Figures 6 and 7, which also show the model and the mesh discretization with a hybrid mesher.

4.4. Acquisition of Datasets. The uniform design method, proposed by mathematicians Kaitai Fang and Yuan Wang, is a type of experimental design from the uniformity and is based on the uniform distribution of the test point within the test range [46]. The essence of all test design methods, including uniform design, is to identify representative points within the experimental data range, with the aim of reducing the workload of the test. The method can select the representative test points from the comprehensive test points and distribute them evenly within the test range, which can reflect the main characteristics of the whole. Compared with the orthogonal design, the uniform design method achieves uniform dispersion and reduces the number of tests but does not achieve neat and comparable characteristics. In particular, when the range of test factors is large and many horizontal tests are needed, the uniform design can achieve the effect as long as the test of the level of the factor is equal to the number of factors, which greatly reduces the workload because the number of orthogonal tests is equal to the horizontal number square test.

To reduce the model computation, the uniform design method is selected when determining the training dataset. As shown in Table 2, the value scheme of five geotechnical parameters is determined by using the uniform design method, and the range of values is shown in Table 1. Using the finite element model constructed in Section 4.3 and the geotechnical parameter scheme in Table 2, the deformation parameters including the vault settlement, BC convergence, and DE convergence of each geotechnical parameter scheme are obtained. The obtained dataset is used as the training data of the back analysis, as shown in Table 2. To test the accuracy of the back analysis neural network obtained by using the training dataset, five sets of data are taken as the testing data, and the displacement deformation value of the feature points is obtained by using the numerical simulation method, as shown in Table 3.

5. Stability Evaluation of the Surrounding Rock

5.1. Construction of the RCGA-ANN. The scheme parameters used as the training set and the measuring point deformations are shown in Table 2. The input data include the three displacement parameters, and the output data include the five geotechnical parameters.

To calculate the weight value of the neural network and to prevent the absolute value of a few data points that are too large from overwhelming the small values in the dataset, all training samples are standardized to a range of −1.0 to 1.0. The dimensional data can be converted into dimensionless data, so that the unequal use of variables of different physical meaning and different dimensions can be avoided. Thus, the link weights range from −1.0 to 1.0. The equation is expressed as equation (11).

$$x' = \frac{x - x_{\text{mean}}}{x_{\max} - x_{\min}}, \tag{11}$$

where x' is the normalized data, x is the original data, $x_{\min}$ is the minimum of the original data, x_{mean} is the mean of the original data, and $x_{\max}$ is the maximum of the original data.

The training data in Table 2 are normalized using the above method, as shown in Table 4. In addition, the normalized calculation rules established by the data in Table 2 are used to normalize the test data in Table 3, and the results are shown in Table 5.

Based on the normalized training dataset (Table 4), the structure of the optimal neural network structure of 3-20-10–5 is trained; that is, the input parameters are 3, the output parameters are 5, and the intermediate implicit layer is 2 layers that contain 20 and 10 nodes collectively. To improve the accuracy of the calculation and avoid the problem of the local optimal value, the RCGA is calculated to determine the connection weight.

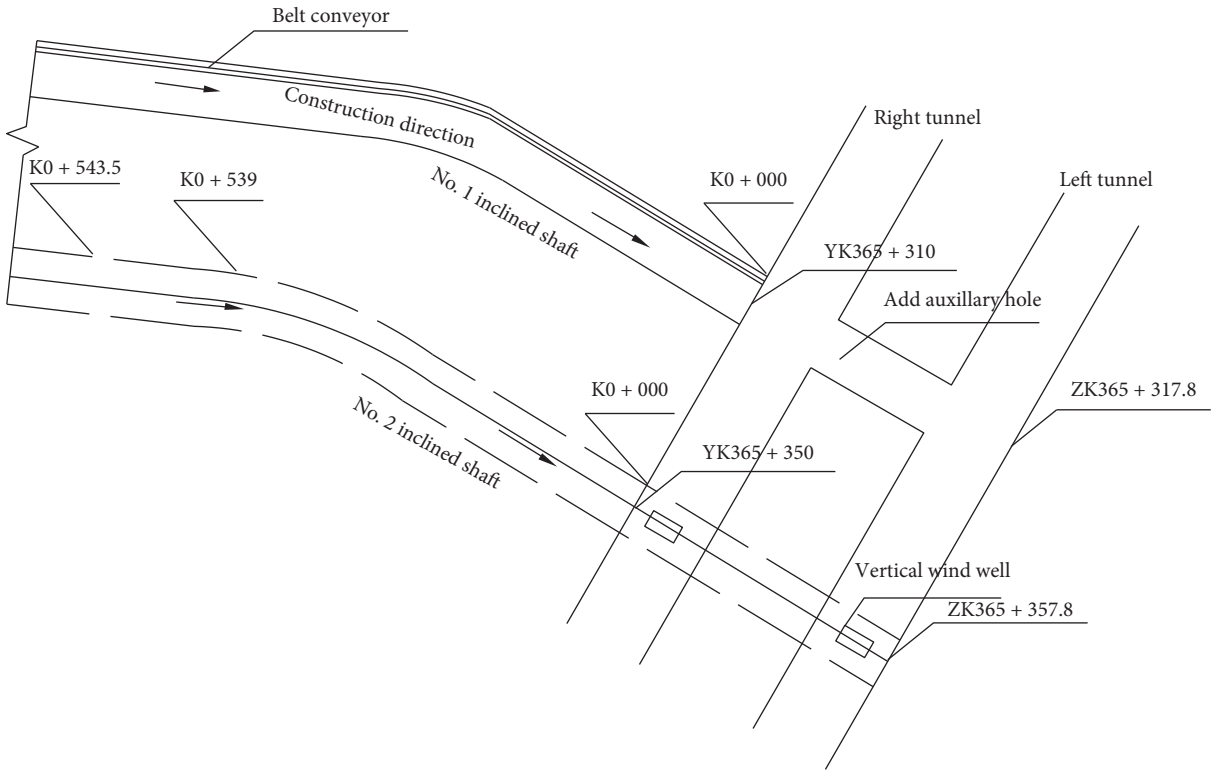

Figure 4: Slope well layout of the Yu Liao Tunnel.

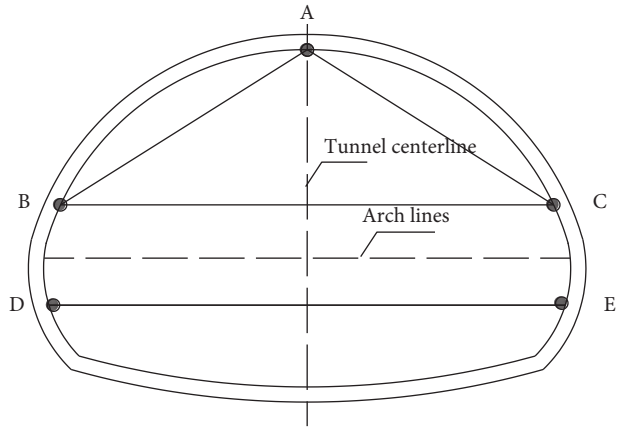

Figure 5: Layout of the monitored points.

Table 1: Material parameters.

Parameters	Unit weight (kN/m^2)	Friction angleφ (°)	Cohesion$c$ (MPa)	Young's modulus E (GPa)	Poisson's ratio μ
Values	22.5–26.5	27–60	0.2–2	1.3–20	0.2–0.35

5.2. Parameters Obtained via Back Analysis. In this section, the field measurement data of the vault settlement and the horizontal convergence of ZK 362 + 400 are used in the back analysis; $A = 6.91$ mm, $BC = 7.23$ mm, and $DE = 1.35$ mm.

Through the above calculation, we obtained the relevant geotechnical parameters of the test point. The proposed strength parameters obtained via back analysis are given as follows: effective friction angle equals 49.5°, effective cohesion equals 104 kPa, unit weight equals 23.6 kN/m^3, Young's modulus equals 3.8 GPa, and Poisson's ratio equals 0.246. By obtaining the initial parameters using the RCGA, the performance is improved and surpasses 100%, as shown in Figure 8.

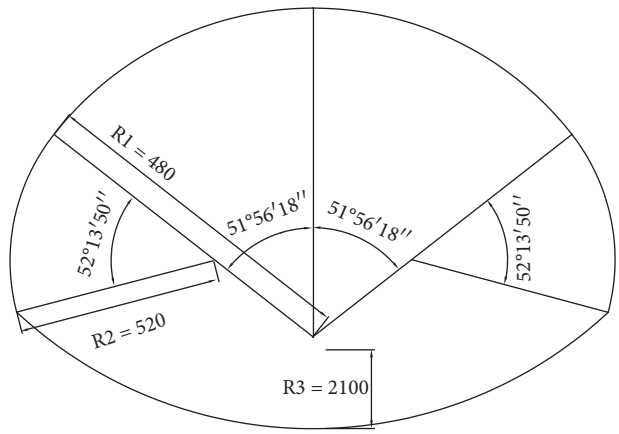

Figure 6: Section of the Yu Liao Tunnel.

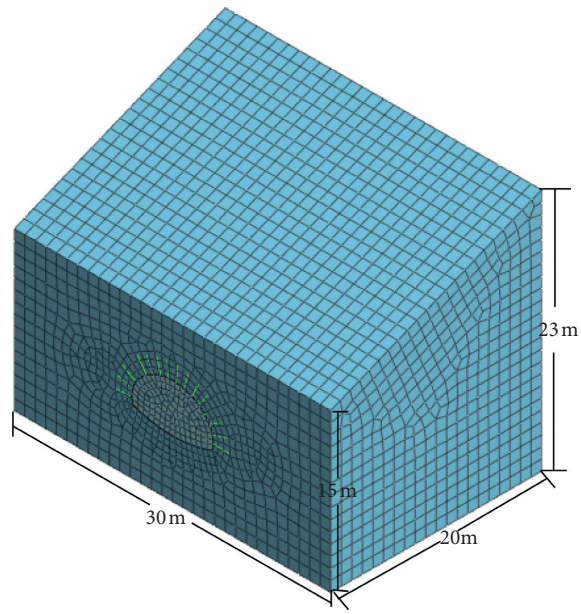

Figure 7: Finite element model size.

Table 2: Scheme parameters based on the uniform design method.

Number	Unit weight (kN/m^2)	φ (°)	c (MPa)	E (GPa)	μ	A vault settlement (mm)	BC convergence (mm)	DE convergence (mm)
1	22.5	32.21	1.211	13.11	0.3184	2.3	0.6	1.6
2	22.71	39.16	2	5.237	0.2789	5.8	0.84	1.48
3	22.92	46.11	1.132	18.03	0.2395	1.7	0.092	0.146
4	23.13	53.05	1.921	10.16	0.2	3.1	0.095	0.2
5	23.34	60	1.053	2.284	0.3263	13.3	4	5.5
6	23.55	30.47	1.842	15.8	0.2868	2	0.34	0.6
7	23.76	37.42	0.9737	7.205	0.2474	4.6	0.3	3.2
8	23.97	44.37	1.763	20	0.2079	1.6	0.02	0.06
9	24.18	51.32	0.8947	12.13	0.3342	2.6	0.82	1.4
10	24.39	58.26	1.684	4.253	0.2947	7.6	1.48	2.6
11	24.61	28.74	0.8158	17.05	0.2553	2.3	0.24	4.2
12	24.82	35.68	1.605	9.174	0.2158	3.7	0.0065	0.0095
13	25.03	42.63	0.7368	1.3	0.3421	25.3	8.9	28.4
14	25.24	49.58	1.526	14.09	0.3026	2.4	0.52	0.88
15	25.45	56.53	0.6579	6.221	0.2632	5.5	0.6	1.02
16	25.66	27	1.447	19.02	0.2237	2	0.012	0.374
17	25.87	33.95	0.5789	11.14	0.35	3.8	3.4	9.9
18	26.08	40.89	1.368	3.268	0.3105	10.5	2.6	4.4
19	26.29	47.84	0.5	16.06	0.2711	2.3	0.64	2.6
20	26.5	54.79	1.289	8.189	0.2316	4.4	0.158	0.22

Table 3: Testing set.

Number	Unit weight (kN/m^2)	φ (°)	c (MPa)	E (GPa)	μ	A vault settlement (mm)	BC convergence (mm)	DE convergence (mm)
1	26.3	34	1.211	11.15	0.32	3.2	0.82	2.86
2	22.71	40	1.5	10.16	0.28	2.05	0.307	0.52
3	25.5	43.2	1.15	18.03	0.28	1.9	0.287	0.5
4	23.5	50	0.92	8.16	0.29	3.9	0.684	1.175
5	23.8	47.84	1.053	2.284	0.3263	13.7	3.97	6.6

Table 4: The normalized training dataset.

Number	Unit weight		c	E	μ	A vault settlement	BC convergence	DE convergence
1	−1.0000	−0.6842	−0.0520	0.2631	0.5787	−0.9409	−0.8665	−0.8880
2	−0.8950	−0.2630	1.0000	−0.5789	0.0520	−0.6456	−0.8126	−0.8964
3	−0.7900	0.1582	−0.1573	0.7893	-0.4733	−0.9916	−0.9808	−0.9904
4	−0.6850	0.5788	0.8947	−0.0524	-1.0000	−0.8734	−0.9801	−0.9866
5	−0.5800	1.0000	−0.2627	−0.8948	0.6840	−0.0127	−0.1019	−0.6132
6	−0.4750	−0.7897	0.7893	0.5508	0.1573	−0.9662	−0.9250	−0.9584
7	−0.3700	−0.3685	−0.3684	−0.3684	-0.3680	−0.7468	−0.9340	−0.7752
8	−0.2650	0.0527	0.6840	1.0000	-0.8947	−1.0000	−0.9970	−0.9964
9	−0.1600	0.4739	−0.4737	0.1583	0.7893	−0.9156	−0.8171	−0.9020
10	−0.0550	0.8945	0.5787	−0.6842	0.2627	−0.4937	−0.6686	−0.8175
11	0.0550	−0.8945	−0.5789	0.6845	-0.2627	−0.9409	−0.9475	−0.7048
12	0.1600	−0.4739	0.4733	−0.1579	-0.7893	−0.8228	−1.0000	−1.0000
13	0.2650	−0.0527	−0.6843	−1.0000	0.8947	1.0000	1.0000	1.0000
14	0.3700	0.3685	0.3680	0.3679	0.3680	−0.9325	−0.8845	−0.9387
15	0.4750	0.7897	−0.7895	−0.4737	-0.1573	−0.6709	−0.8665	−0.9288
16	0.5800	−1.0000	0.2627	0.8952	-0.6840	−0.9662	−0.9988	−0.9743
17	0.6850	−0.5788	−0.8948	0.0524	1.0000	−0.8143	−0.2369	−0.3033
18	0.7900	−0.1582	0.1573	−0.7895	0.4733	−0.2489	−0.4168	−0.6907
19	0.8950	0.2630	−1.0000	0.5786	-0.0520	−0.9409	−0.8575	−0.8175
20	1.0000	0.6842	0.0520	−0.2632	-0.5787	−0.7637	−0.9659	−0.9852

Table 5: The normalized testing dataset.

Number	Unit weight	φ	c	E	μ	A vault settlement	BC convergence	DE convergence
1	0.9000	−0.5758	−0.0520	0.0535	0.6000	−0.8650	−0.8171	−0.7992
2	−0.8950	−0.2121	0.3333	-0.0524	0.0667	−0.9620	−0.9324	−0.9640
3	0.5000	−0.0182	−0.1333	0.7893	0.0667	−0.9747	−0.9369	−0.9654
4	−0.5000	0.3939	−0.4400	-0.2663	0.2000	−0.8059	−0.8476	−0.9179
5	−0.3500	0.2630	−0.2627	-0.8948	0.6840	0.0211	−0.1087	−0.5357

5.3. Stability Evaluation of the Surrounding Rock. After obtaining the parameters of the surrounding rock, the ODSRM is used to calculate the safety factor to evaluate the stability of the surrounding rock. As shown in Table 6, $\Delta = 0.1$, and the cohesion and friction angle are reduced one by one.

The geotechnical parameters in the FEM (Figure 8) are obtained in Section 4 via the RCGA-ANN. In the first reduction step, denoted as *S1*, the parameters are set to $\varphi = 49.5^\circ$ and $c = 104$ kPa; then, the vault settlement is calculated. Calculation steps numbers 2, 3, and 4 are the cohesion reduction step, friction angle reduction step, and combined reduction step, respectively. According to the comparison of the vault settlement of steps numbers 2, 3, and 4, the sequence number of *S2* is number 4. The reduction is performed until the vault settlement has a significant increase. After 25 reduction iterations, the process with $\Delta = 0.1$ is terminated; then, the result of the safety factor of section $F_s = 2.06$ is obtained, as shown in Figure 9.

Through the process with $\Delta = 0.05$ in the ODSRM, $\Delta = 0.2$ in the ODSRM, and $\Delta = 0.1$ in the SRM, as shown in Figures 10–12, we obtained $F_s = 2.08$, $F_s = 2.03$, and $F_s = 2.19$, respectively, as illustrated in Figures 10–12 and Table 7.

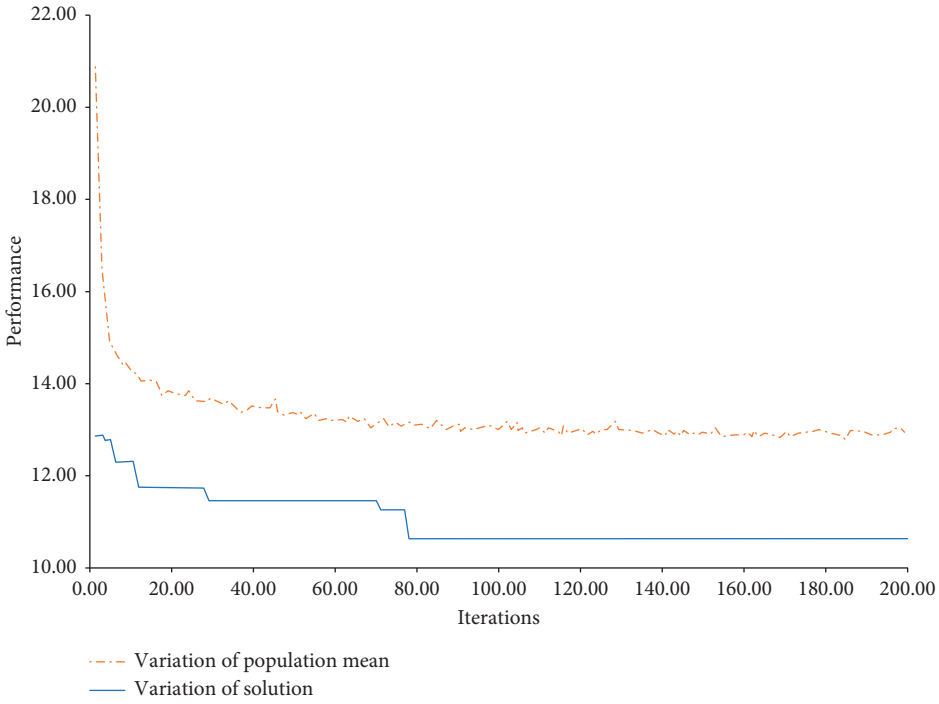

Figure 8: Perturbation with iterations.

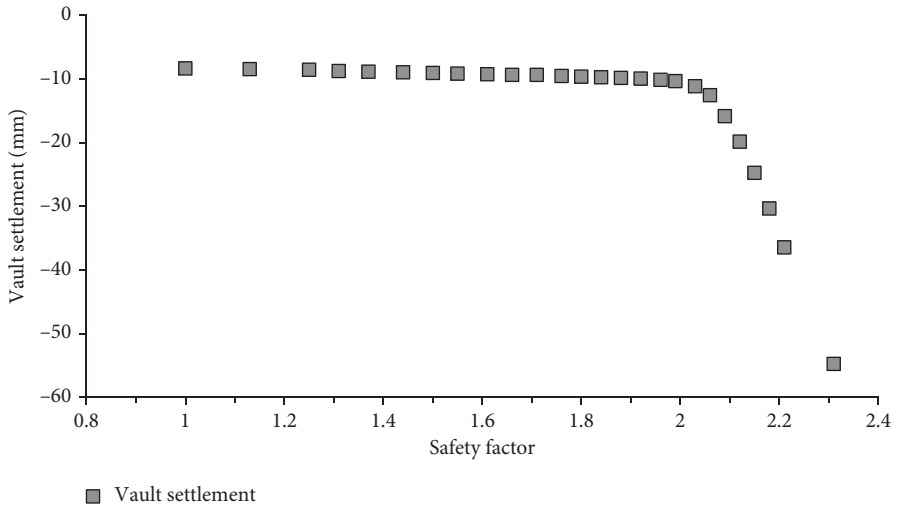

Figure 9: Reduction ratio equal to 0.1 in the ODSRM.

According to the comparative analysis of the four conditions, we obtain two results. First, the safety factor gained by using the ODSRM is smaller than that obtained by using the SRM with the same reduction factors; i.e., the SRM overestimates safety. Second, the reduction factor can affect the safety factor because, when a reduction factor is too high, it could result in a suboptimal selection of one of the two reduction parameters.

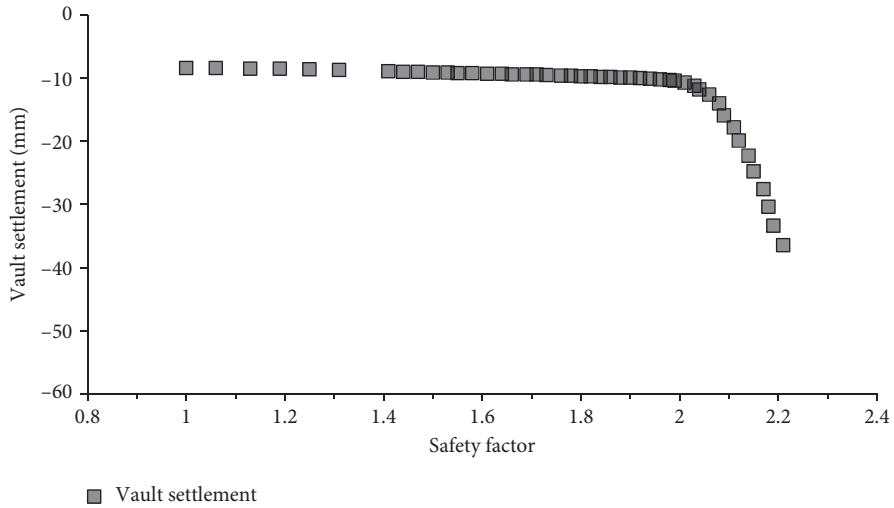

Figure 10: Reduction ratio equal to 0.05 in the ODSRM.

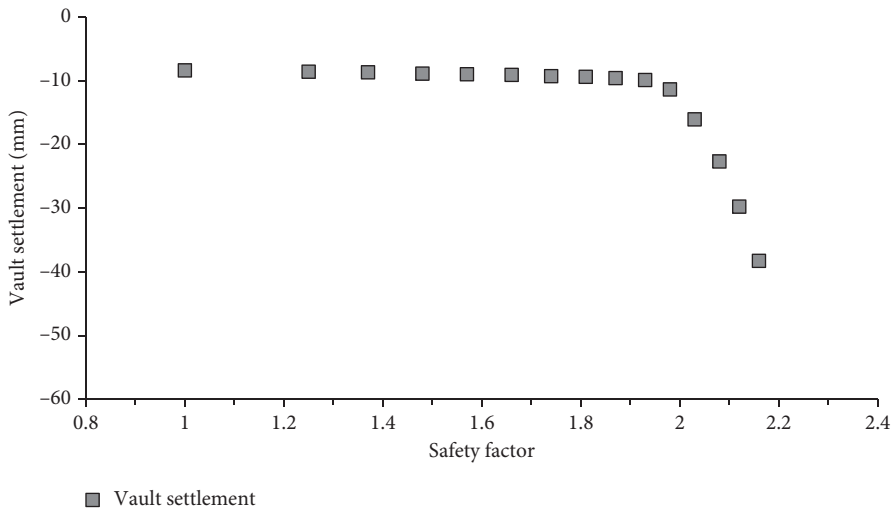

Figure 11: Reduction ratio equal to 0.2 in the ODSRM.

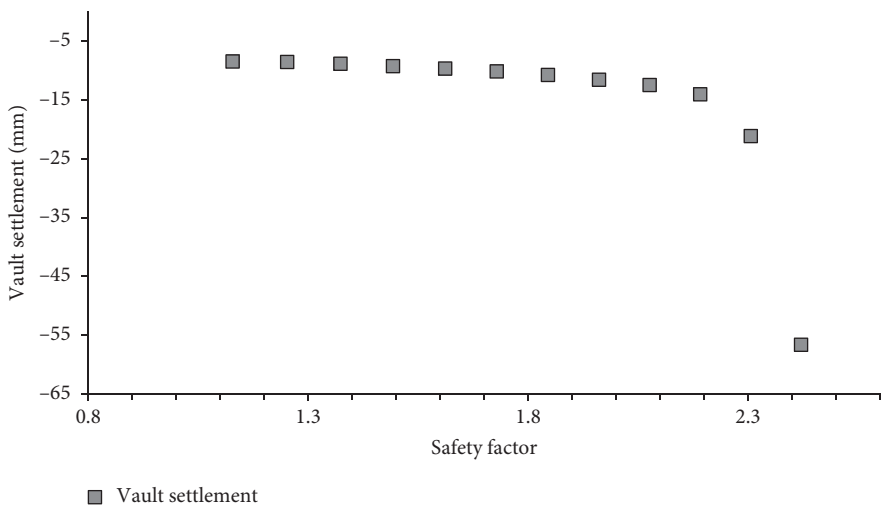

Figure 12: Reduction ratio equal to 0.1 in the SRM.

Table 6: Reduction ratio equal to 0.1.

Number	Sequence number	φ	c	Vault settlement mm	k_1	k_2	F_s
1		49.5	104	−8.4	1.00	1.00	1.00
2	*S1*	49.5	94.55	−8.4	1.10	1.00	1.06
3		45	104	−8.4	1.00	1.10	1.06
4	*S2*	45	94.55	−8.5	1.10	1.10	1.13
5	*S3*	41.25	86.67	−8.6	1.20	1.20	1.25
6		41.25	80	−8.7	1.30	1.20	1.31
7	*S4*	38.08	86.67	−8.8	1.20	1.30	1.31
8	*S5*	38.08	80	−8.9	1.30	1.30	1.37
9		35.35	80	−9.1	1.30	1.40	1.42
10	*S6*	38.08	74.29	−9	1.40	1.30	1.44
11		35.35	74.29	−9.3	1.40	1.40	1.49
12	*S7*	38.08	69.33	−9.1	1.50	1.30	1.50
13		35.35	69.33	−9.4	1.50	1.40	1.56
14	*S8*	38.08	65	−9.2	1.60	1.30	1.55
15		35.35	65	−9.5	1.60	1.40	1.62
16	*S9*	38.08	61.18	−9.3	1.70	1.30	1.61
17		35.35	61.18	−9.6	1.70	1.40	1.68
18	*S10*	38.08	57.78	−9.4	1.80	1.30	1.66
19		35.35	57.78	−9.8	1.80	1.40	1.74
20	*S11*	38.08	54.74	−9.4	1.90	1.30	1.71
21		35.35	54.74	−9.8	1.90	1.40	1.79
22	*S12*	38.08	52	−9.6	2.00	1.30	1.76
23		35.35	52	−10	2.00	1.40	1.84
24	*S13*	38.08	49.52	−9.7	2.10	1.30	1.80
25		35.35	49.52	−10.2	2.10	1.40	1.89
26	*S14*	38.08	47.27	−9.8	2.20	1.30	1.84
27		35.35	47.27	−10.3	2.20	1.40	1.94
28	*S15*	38.08	45.22	−9.9	2.30	1.30	1.88
29		35.35	45.22	−10.5	2.30	1.40	1.98
30	*S16*	38.08	43.33	−10	2.40	1.30	1.92
31		35.35	43.33	−10.7	2.40	1.40	2.02
32	*S17*	38.08	41.6	−10.2	2.50	1.30	1.96
33		35.35	41.6	−11.4	2.50	1.40	2.06
34	*S18*	38.08	40	−10.4	2.60	1.30	1.99
35		35.35	40	−12.8	2.60	1.40	2.10
36	*S19*	38.08	38.52	−11.2	2.70	1.30	2.03
37		35.35	38.52	−16.9	2.70	1.40	2.14
38	*S20*	38.08	37.14	−12.6	2.80	1.30	2.06
39		35.35	37.14	−20.9	2.80	1.40	2.18
40	*S21*	38.08	35.86	−15.9	2.90	1.30	2.09
41		35.35	35.86	−27.6	2.90	1.40	2.21
42	*S22*	38.08	34.67	−19.9	3.00	1.30	2.12
43		35.35	34.67	−35.5	3.00	1.40	2.25
44	*S23*	38.08	33.54	−24.8	3.10	1.30	2.15
45		35.35	33.54	−44.3	3.10	1.40	2.28
46	*S24*	38.08	32.5	−30.4	3.20	1.30	2.18
47		35.35	32.5	−54.8	3.20	1.40	2.31
48	*S25*	38.08	31.52	−36.5	3.30	1.30	2.21

Table 7: Safety factors under various reduction factors.

Number	Method	Reduction factor	φ'	c'	F_s
1		0.05	38.08	36.49	2.08
2	ODSRM	0.1	38.08	37.14	2.06
3		0.2	41.25	32.5	2.03
4	SRM	0.1	24.75	52	2.19

6. Conclusions

In conclusion, a new double-strength reduction method, called the optimization double-strength reduction method (ODSRM), is proposed and verified. The proposed method can reduce the cohesion and friction angle by different reduction factors. The ODSRM is applied in the Yu Liao Tunnel, where it is demonstrated that the combined method can use the measured displacements to obtain the safety factor. Through the establishment of a numerical model, the vault and the horizontal convergence under different values of various parameters are calculated. The calculated data are divided into the training and testing dataset, and the proposed method is used to get the parameters of the neural network. And then the safety factor can be calculated. Compared with the previous SRM, the ODSRM can consider the different effects of these parameters and avoid overestimating the safety factor.

Data Availability

The experimental data used to support the findings of this study are included within the article.

Conflicts of Interest

The authors declare no conflicts of interest.

Acknowledgments

The authors gratefully acknowledge the support provided by the National Natural Science Foundation of China (Grant nos. 71771020 and 71631007), and Financial Project of Beijing Municipal Engineering Research Institute (Grant no J-21051-270).

References

[1] A. Paternesi, H. F. Schweiger, and G. Scarpelli, "Numerical analyses of stability and deformation behavior of reinforced and unreinforced tunnel faces," *Computers and Geotechnics*, vol. 88, pp. 256–266, 2017.

[2] T. Matsui and K.-C. San, "Finite element slope stability analysis by shear strength reduction technique," *Soils and Foundations*, vol. 32, no. 1, pp. 59–70, 1992.

[3] L. Pantelidis and D. Griffiths, "Stability assessment of slopes using different factoring strategies," *Journal of Geotechnical and Geoenvironmental Engineering*, vol. 138, pp. 1158–1160, 2011.

[4] B. Schneider-Muntau, G. Medicus, and W. Fellin, "Strength reduction method in Barodesy," *Computers and Geotechnics*, vol. 95, pp. 57–67, 2018.

[5] F. Tschuchnigg, H. F. Schweiger, and S. W. Sloan, "Slope stability analysis by means of finite element limit analysis and finite element strength reduction techniques. Part I: numerical studies considering non-associated plasticity," *Computers and Geotechnics*, vol. 70, pp. 169–177, 2015.

[6] F. Tschuchnigg, H. F. Schweiger, and S. W. Sloan, "Slope stability analysis by means of finite element limit analysis and finite element strength reduction techniques. Part II: back analyses of a case history," *Computers and Geotechnics*, vol. 70, pp. 178–189, 2015.

[7] K. Shilei, Y. Feng, and J. Zhang, "Finite element upper bound analysis of stability of unlined elliptical tunnel based on strength reduction method," *Journal of Hunan University: Natural Sciences*, vol. 42, pp. 104–109, 2015.

[8] J. Qiao, Y. Zhang, J. Gao, and Y. Li, "Application of strength reduction method to stability analysis of shield tunnel face," *Journal of Tianjin University*, vol. 43, pp. 14–20, 2010.

[9] J. Li, J. Si, H. Zhong, and R. Zhao, "Application of strength reduction method to stability analysis of shield tunnel face," *China Civil Engineering Journal*, vol. 50, pp. 199–202, 2017.

[10] J. Sun, B. Liu, Z. Chu, L. Chen, X. Li, and X. Li, "Tunnel collapse risk assessment based on multistate fuzzy Bayesian networks," *Quality and Reliability Engineering International*, vol. 34, no. 8, pp. 1646–1662, 2018.

[11] O. C. Zienkiewicz, C. Humpheson, and R. W. Lewis, "Associated and non-associated visco-plasticity and plasticity in soil mechanics," *Géotechnique*, vol. 25, no. 4, pp. 671–689, 1975.

[12] R. L. Michalowski, "Slope stability analysis: a kinematical approach," *Géotechnique*, vol. 45, no. 2, pp. 283–293, 1995.

[13] D. Naylor, *Finite Elements and Slope Stability*, Springer, Berlin, Germany, 1982.

[14] D. Taylor, *Fundamentals of Soil Mechanics*, Chapman And Hall, Limited., New York, NY, USA, 1948.

[15] F. Tang, Y. Zheng, and S. Zhao, "Discussion on two safety factors for progressive failure of soil slope," *Yanshilixue Yu Gongcheng Xuebao/Chinese Journal of Rock Mechanics and Engineering*, vol. 26, pp. 1402–1407, 2007.

[16] C. Li, W. Zhu, X. Lu, and P. Cui, "Studied on landslide translating into debris-flow under rainfall," *China Civil Engineering Journal*, vol. 43, pp. 499–505, 2010.

[17] Z. Chu, Z. Wu, Q. Liu, and B. Liu, "Analytical solution for lined circular tunnels in deep viscoelastic Burgers rock considering the longitudinal discontinuous excavation and sequential installation of liners," *Journal of Engineering Mechanics (ASCE)*, vol. 147, no. 4, pp. 1–22, 2021.

[18] A. Isakov and Y. Moryachkov, "Estimation of slope stability using two-parameter criterion of stability," *International Journal of Geomechanics*, vol. 14, Article ID 06014004, 2013.

[19] W. Wang, J. Zou, X. Zhang, and H. Zhang, "Research on the existence of the shortest path of strength reduction in the limit analysis of shallow buried tunnel," *Journal of Hunan University (Natural Sciences)*, vol. 44, pp. 151–157, 2017.

[20] W. Yuan, B. Bai, X.-C. Li, and H.-B. Wang, "A strength reduction method based on double reduction parameters and its application," *Journal of Central South University*, vol. 20, no. 9, pp. 2555–2562, 2013.

[21] B. Bai, W. Yuan, and X.-C. Li, "A new double reduction method for slope stability analysis," *Journal of Central South University*, vol. 21, no. 3, pp. 1158–1164, 2014.

[22] W. Gao and M. Ge, "Back analysis of rock mass parameters and initial stress for the Longtan tunnel in China," *Engineering with Computers*, vol. 32, no. 3, pp. 497–515, 2016.

[23] D. E. L. Ong and C. S. Choo, "Back-analysis and finite element modeling of jacking forces in weathered rocks," *Tunnelling and Underground Space Technology*, vol. 51, pp. 1–10, 2016.

[24] P. Oreste, "Back-analysis techniques for the improvement of the understanding of rock in underground constructions," *Tunnelling and Underground Space Technology*, vol. 20, no. 1, pp. 7–21, 2005.

[25] S. Sakurai and K. Takeuchi, "Back analysis of measured displacements of tunnels," *Rock Mechanics and Rock Engineering*, vol. 16, no. 3, pp. 173–180, 1983.

[26] Y. J. Shang, J. G. Cai, W. D. Hao, X. Y. Wu, S. H. Li, and S. Li, "Intelligent back analysis of displacements using precedent type analysis for tunneling," *Tunnelling and Underground Space Technology*, vol. 17, no. 4, pp. 381–389, 2002.

[27] L. Q. Zhang, Z. Q. Yue, Z. F. Yang, J. X. Qi, and F. C. Liu, "A displacement-based back-analysis method for rock mass modulus and horizontal in situ stress in tunneling - illustrated with a case study," *Tunnelling and Underground Space Technology*, vol. 21, no. 6, pp. 636–649, 2006.

[28] M. Yazdani, M. Sharifzadeh, K. Kamrani, and M. Ghorbani, "Displacement-based numerical back analysis for estimation of rock mass parameters in Siah Bisheh powerhouse cavern using continuum and discontinuum approach," *Tunnelling and Underground Space Technology*, vol. 28, pp. 41–48, 2012.

[29] M. Sharifzadeh, A. Tarifard, and M. A. Moridi, "Time-dependent behavior of tunnel lining in weak rock mass based on displacement back analysis method," *Tunnelling and Underground Space Technology*, vol. 38, pp. 348–356, 2013.

[30] K. Zhang, W. Zheng, C. Xu, and S. Chen, "An improved extension system for assessing risk of water inrush in tunnels in carbonate karst terrain," *KSCE Journal of Civil Engineering*, vol. 23, no. 5, pp. 2049–2064, 2019.

[31] S. Grossberg, "Nonlinear neural networks: principles, mechanisms, and architectures," *Neural Networks*, vol. 1, no. 1, pp. 17–61, 1988.

[32] X.-T. Feng, Z. Zhang, and Q. Sheng, "Estimating mechanical rock mass parameters relating to the Three Gorges Project permanent shiplock using an intelligent displacement back analysis method," *International Journal of Rock Mechanics and Mining Sciences*, vol. 37, no. 7, pp. 1039–1054, 2000.

[33] K. Zhang, D. D. Tannant, W. Zheng, S. Chen, and X. Tan, "Prediction of karst for tunnelling using fuzzy assessment combined with geological investigations," *Tunnelling and Underground Space Technology*, vol. 80, pp. 64–77, 2018.

[34] C. Z. Janikow and Z. Michalewicz, "An experimental comparison of binary and floating point representations in genetic algorithms," in *Proceedings of the 4th ICGA*, pp. 31–36, San Diego, CA, USA, July 1991.

[35] B. Pichler, R. Lackner, and H. A. Mang, "Back analysis of model parameters in geotechnical engineering by means of soft computing," *International Journal for Numerical Methods in Engineering*, vol. 57, no. 14, pp. 1943–1978, 2003.

[36] L. Kaiyun, Q. Chunsheng, and L. Baoguo, "Research on elastoplastic displacement back analysis method based on GA-GRNN algorithm in three-dimension of Wushi tunnel," *Rock and Soil Mechanics*, vol. 30, pp. 1805–1809, 2009.

[37] Y.-P. Guan, J. Song, Y.-P. WANG, and Y. Liu, "Back analysis of mechanical parameters of surrounding rocks based on GA-BP algorithm," *Journal of Northeastern University (Natural Science)*, vol. 33, pp. 276–278, 2012.

[38] H. Ji, Y.-F. Jin, Z.-Y. Yin, Z.-X. Wu, and S.-L. Shen, "Enhance of genetic algorithm and its application to the identification of soil parameters by inverse analysis *Chinese*," *Journal of Computational Mechanics*, vol. 35, pp. 224–229, 2018.

[39] Y.-C. Chuang, C.-T. Chen, and C. Hwang, "A real-coded genetic algorithm with a direction-based crossover operator," *Information Sciences*, vol. 305, pp. 320–348, 2015.

[40] R. B. Agrawal, K. Deb, and R. Agrawal, "Simulated binary crossover for continuous search space," *Complex Systems*, vol. 9, pp. 115–148, 1995.

[41] H.-C. Kuo and C.-H. Lin, "A directed genetic algorithm for global optimization," *Applied Mathematics and Computation*, vol. 219, no. 14, pp. 7348–7364, 2013.

[42] K. Deb, A. Pratap, S. Agarwal, and T. Meyarivan, "A fast and elitist multiobjective genetic algorithm: nsga-II," *IEEE Transactions on Evolutionary Computation*, vol. 6, no. 2, pp. 182–197, 2002.

[43] Y. Cheng, Z. Zhao, and J. Wang, "Realization of Pan Jiazheng's extremum principle with optimization methods," *Chinese Journal of Rock Mechanics and Engineering*, vol. 27, pp. 782–788, 2008.

[44] A. C. Rios-Coelho, W. F. Sacco, and N. Henderson, "A Metropolis algorithm combined with Hooke-Jeeves local search method applied to global optimization," *Applied Mathematics and Computation*, vol. 217, no. 2, pp. 843–853, 2010.

[45] B. Bai, W. Yuan, L. Shi, and J. X. Li, "Comparing a new double reduction method to classic strength reduction method for slope stability analysis," *Rock and Soil Mechanics*, vol. 36, pp. 1275–1281, 2015.

[46] X. Li, X. Li, and Y. Su, "A hybrid approach combining uniform design and support vector machine to probabilistic tunnel stability assessment," *Structural Safety*, vol. 61, pp. 22–42, 2016.